

# Nucleolin-Targeting AS1411 Aptamer-Modified Micelle for the Co-Delivery of Doxorubicin and miR-519c to Improve the Therapeutic Efficacy in Hepatocellular Carcinoma Treatment

This article was published in the following Dove Press journal:  
*International Journal of Nanomedicine*

Xiao Liang\*  
Yudi Wang\*  
Hui Shi  
Mengmeng Dong  
Haobo Han   
Quanshun Li 

Key Laboratory for Molecular Enzymology and Engineering of Ministry of Education, School of Life Sciences, Jilin University, Changchun, 130012, People's Republic of China

\*These authors contributed equally to this work

**Background:** Multidrug resistance (MDR) has emerged to be a major hindrance in cancer therapy, which contributes to the reduced sensitivity of cancer cells toward chemotherapeutic drugs mainly owing to the over-expression of drug efflux transporters. The combination of gene therapy and chemotherapy has been considered as a potential approach to improve the anti-cancer efficacy by reversing the MDR effect.

**Materials and Methods:** The AS1411 aptamer-functionalized micelles were constructed through an emulsion/solvent evaporation strategy for the simultaneous co-delivery of doxorubicin and miR-519c. The therapeutic efficacy and related mechanism of micelles were explored based on the in vitro and in vivo active targeting ability and the suppression of MDR, using hepatocellular carcinoma cell line HepG2 as a model.

**Results:** The micelle was demonstrated to possess favorable cellular uptake and tumor penetration ability by specifically recognizing the nucleolin in an AS1411 aptamer-dependent manner. Further, the intracellular accumulation of doxorubicin was significantly improved due to the suppression of ABCG2-mediated drug efflux by miR-519c, resulting in the efficient inhibition of tumor growth.

**Conclusion:** The micelle-mediated co-delivery of doxorubicin and miR-519c provided a promising strategy to obtain ideal anti-cancer efficacy through the active targeting function and the reversion of MDR.

**Keywords:** micelle, aptamer, nucleolin, multidrug resistance, tumor targeting

## Introduction

Chemotherapy has been widely accepted to be the primary strategy in the treatment of hepatocellular carcinoma (HCC), exhibiting significant therapeutic efficacy in the clinic.<sup>1,2</sup> However, it still suffers from undesirable side effects, such as systemic toxicity, short half-life and lack of precise targets.<sup>3-5</sup> Especially, the occurrence of multidrug resistance (MDR) of cancer cells can reduce the efficacy of chemotherapeutic drugs,<sup>6,7</sup> which has become the most crucial reason for the failure of HCC treatment. The phenomenon was mainly attributed to the over-expression of ATP-binding cassette (ABC) transporter family in cancer cells, including ABCG1, ABCC1 and ABCG2.<sup>8-10</sup> Among them, ABCG2, one of the initially discovered transporters, plays an important role in the ABC-dependent drug efflux, and is capable of transporting a broad range of chemotherapeutic agents such as paclitaxel

Correspondence: Quanshun Li; Haobo Han  
Tel/Fax +86-431-85155200  
Email quanshun@jlu.edu.cn;  
hanhaobo@jlu.edu.cn

and doxorubicin (DOX), thus conferring the drug resistance and further leading to high recurrence and poor survival of patients bearing HCC.<sup>11–13</sup> Therefore, to block ABCG2-mediated drug efflux by inhibiting the ABCG2 expression could efficiently reverse MDR in the carcinogenesis and enhance the sensitivity of cancer cells to chemotherapeutics.<sup>14</sup> Non-coding microRNAs (miRNAs) can post-transcriptionally regulate the mRNA expression by targeting the 3'-UTR region, and thus play a significant role in various cellular functions such as differentiation, proliferation and apoptosis.<sup>15,16</sup> Differential expression of miRNAs has emerged to be vital regulators of MDR acquisition in HCC progression,<sup>17,18</sup> where miR-519c has been demonstrated to be highly associated with the reversion of MDR by targeting the ABCG2 mRNA.<sup>19–21</sup> Owing to its down-regulated expression in cancer cells, the combination of chemotherapy and miR-519c delivery exhibited great potential in the synergistic HCC therapy by overcoming the MDR and further enhancing the cells' sensitivity to chemotherapeutic drugs.<sup>22</sup>

To achieve the maximal efficiency of combinational therapy, the development of efficient and safe nanocarriers is highly required.<sup>23–26</sup> Up to now, a variety of carriers have been investigated for the co-delivery of drugs and genes/photosensitizers in anti-cancer trails, including cationic polymers, liposomes, human serum albumin, hydrogels and inorganic nanoparticles.<sup>27–33</sup> Among them, polymeric micelles formed by amphiphilic block copolymers have gained more attention due to their unique properties such as the core/shell structure, excellent stability, and ideal encapsulation and delivery efficiency of hydrophobic drugs.<sup>34–37</sup> Polyethylene glycol-polylactic acid (PEG-PLA), one of the most prominent amphiphilic block copolymers, can self-assemble into micelles with core/shell structure in aqueous phase.<sup>38</sup> Also, the hydrophilic shell on the surface of PEG-PLA micelles is capable of hindering the adsorption of plasma proteins and avoiding the elimination by reticuloendothelial system, resulting in prolonged residence time in circulation system.<sup>39</sup> The nanosized structure of micelles contributes to the diffusion of micelles through the leaky blood vessels to accumulate drugs in the tumor tissues, also known as enhanced permeability and retention (EPR) effect.<sup>40,41</sup> Besides, the characteristics of excellent biodegradability and low toxicity will facilitate their wide applications in drug or gene delivery.<sup>42</sup>

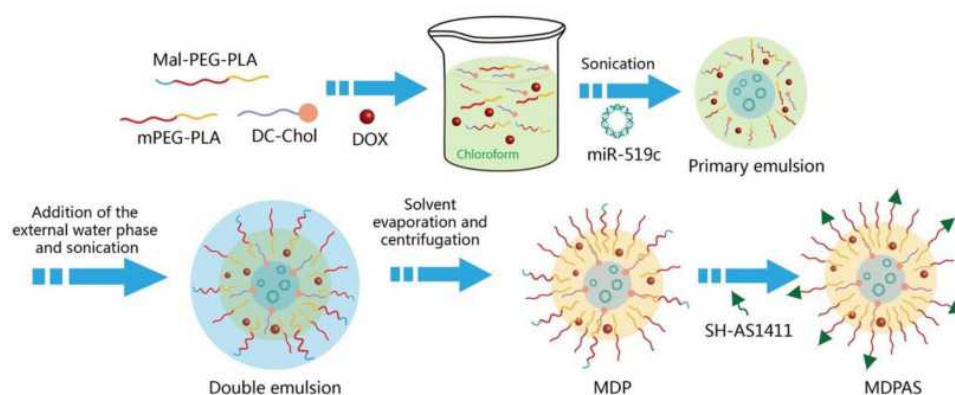
Nevertheless, the micelles are still unsatisfactory to fulfill the requirements in clinical applications due to their limited cellular uptake efficiency and lack of tumor-targeting ability. Thus, the modification of micelles has been widely explored using tumor-targeting ligands including peptides and antibodies.<sup>43,44</sup> Aptamers, also called “chemical antibodies”, are short DNA/RNA oligonucleotides and selected by SELEX technology based on nucleic acid libraries, which can specifically recognize various targets.<sup>45,46</sup> Owing to the unique characteristics such as precise selectivity and high binding affinity, aptamers have been used to enhance the targeting ability of nanoparticles in drug/gene delivery.<sup>46</sup> AS1411, a 26-mer DNA oligonucleotide, has been systemically evaluated in Phase II clinical trial for leukemia treatment.<sup>47</sup> Recently, AS1411 was reported to possess a specific interaction with nucleolin, an important biomarker in various cancer cells to promote the tumor growth and metastasis.<sup>48,49</sup> Thus, the modification of micelles with AS1411 will dramatically facilitate the drug delivery by recognizing the tumor cells via active targeting.

Herein, AS1411 aptamer-functionalized PEG-PLA micelles were constructed through an emulsion/solvent evaporation strategy for the co-delivery of DOX and miR-519c, namely MDPAS (Scheme 1). The therapeutic efficacy and related mechanism of micelles in the cancer treatment were explored based on the active targeting ability and the suppression of MDR, using hepatocellular carcinoma cell line HepG2 as a model.

## Materials and Methods

### Materials

AS1411 aptamer (5'-GGTGGTGGTGGTTGTGGTGGTG GTGG-3') was ordered from Sangon Biotech. (Shanghai, China). The miR-519c expression plasmid was synthesized by GenePharma (Soochow, China). DC-cholesterol (DC-Chol), maleimide (Mal)-PEG<sub>5K</sub>-PLA<sub>21K</sub> and mPEG<sub>5K</sub>-PLA<sub>10K</sub> were purchased from Daigang Biomaterials Co. (Shandong, China). Doxorubicin hydrochloride (>99% purity) was provided by Huafeng Biotech. Co. (Beijing, China). Polyvinyl alcohol (PVA), 3-(4,5-dimethylthiazol-2-yl)-2,5-diphenyltetrazolium bromide (MTT) and tris(2-carboxyethyl)phosphine (TCEP) were purchased from Aladdin (Shanghai, China). 4,6-Diamidino-2-phenylindole (DAPI) and triethylamine were provided by Amresco (Solon, OH). Dulbecco's modified Eagle's medium (DMEM), fetal bovine serum (FBS)



**Scheme 1** The illustration of micelle preparation.

and PBS buffer were purchased from Gibco (Grand Island, NY). LysoTracker<sup>TM</sup> Green dye and LIVE/DEAD<sup>®</sup> Viability/Cytotoxicity kit were purchased from ThermoFisher (Carlsbad, CA). Quant-iT<sup>TM</sup> Pico Green dsDNA assay kit was obtained from Invitrogen (Auckland, NZ). Cell cycle and apoptosis detection kits were provided by BestBio (Shanghai, China). The corresponding caspase activity assay kits and in situ TUNEL detection kit were ordered from Promega (Madison, WA). The primary antibodies against nucleolin, procaspase-3, procaspase-8, procaspase-9, ABCG2, Ki67 and  $\beta$ -actin, and the horseradish peroxidase (HRP)-conjugated secondary antibody were purchased from Abcam (Shanghai, China). TRAzol Universal reagent for RNA isolation was purchased from TIANGEN (Beijing, China). PrimeScript<sup>TM</sup> RT-PCR kit and SYBR<sup>®</sup> Premix Ex Taq<sup>TM</sup> PCR kit were purchased from TaKaRa (Dalian, China). Other reagents were purchased with the highest grade and used without further purification.

## Preparation of MDPAS Micelles

Micelles were prepared by an emulsion/solvent evaporation method, as shown in [Scheme 1](#). Briefly, DC-Chol (1.0 mg), Mal-PEG<sub>5K</sub>-PLA<sub>21K</sub> (2.5 mg) and mPEG<sub>5K</sub>-PLA<sub>10K</sub> (22.5 mg) were dissolved in 0.5 mL chloroform. Doxorubicin hydrochloride (2.5 mg) and triethylamine (3.0  $\mu$ L) were then added into the solution, and the sample was stirred at 4 °C overnight in the dark to achieve the dehydrochlorination and the encapsulation of DOX. The miR-519c plasmid diluted by ultrapure water (1500 ng/ $\mu$ L, 25  $\mu$ L) was gently mixed with the solution, followed by the sonication at 80 W for 2 min. The mixture was added into 5.0 mL of PVA solution (0.1%, w/v) and allowed to sonicate at 80 W for 4 min in an ice bath. Afterward, the

products were transferred into 25 mL of PVA solution (0.3%, w/v) and shaken for 3 h to remove chloroform. Finally, the sample was subjected to the centrifugation at 30,000 g for 1 h (4 °C) to obtain the MDP micelles, which were washed with distilled water twice. For the preparation of MDPAS micelles, AS1411 aptamer (OD<sub>260</sub> of 2.0) was dissolved in 10 mL of TCEP solution (10 mM) and stirred at 4 °C for 2 h. The prepared MDP micelles were re-suspended in the aptamer solution, and the reaction was carried out by the incubation at 4 °C overnight in the dark. The MDPAS micelles were collected through the centrifugation (30,000 g, 1 h, 4 °C) and washed with distilled water twice. Alternatively, M (blank micelles), MAS (blank micelles with the modification of AS1411 aptamer), MD (micelles harboring only DOX) and MDAS (micelles harboring DOX with the modification of AS1411 aptamer) were formulated in an identical procedure with the addition of corresponding components.

## Characterization of MDPAS Micelles

Transmission electron microscopy (TEM) images of different micelle formulations were captured on a HITACHI-H800 microscope at an accelerating voltage of 200 kV. Hydrodynamic diameter and zeta potential of micelles were measured by Malvern Nano ZS90 Zetasizer (Malvern, UK). Agarose gel electrophoresis (1.0%) was carried out to detect the conjugation of AS1411 on the surface of MDPAS micelles (120 V, 20 min).

## Loading and Release Analysis of DOX and miR-519c Plasmid

The DOX loading was measured by detecting the absorbance at 492 nm through GF-M3000 microplate reader (Shandong, China), and the loading of miR-519c plasmid

was detected using Quant-iT™ Pico Green dsDNA assay kit. The encapsulation efficiency (EE) and drug loading efficiency (DL) were determined by the following two formulas:

$$EE(\%) = \frac{\text{amount of loaded gene/drug in micelles}}{\text{amount of gene/drug for preparation}} \times 100\%$$

$$DL(\%) = \frac{\text{amount of loaded gene/drug in micelles}}{\text{amount of micelles}} \times 100\%$$

The DOX release from micelles was evaluated by the incubation of micelles in 1 mL of PBS buffer at 37 °C for 7 days. At predetermined time points, the accumulative release of DOX in the supernatant was calculated through the absorbance at 492 nm following the collection of micelles by the centrifugation at 30,000 g for 1 h (4 °C).

## Cellular Uptake and Distribution of MDPAS Micelles

The DOX fluorescence was utilized to assess the cellular uptake efficiency of MDPAS micelles in HepG2 and human hepatocyte L02 cells, which were obtained from the Shanghai Institute of Cell Bank (Shanghai, China). The cells were inoculated in 6-well plates at a density of  $2.5 \times 10^5$  cells/well and cultured overnight, and then incubated with 1 mL of FBS-free medium containing free DOX, MDP and MDPAS micelles for 6 h, followed by the analysis on a flow cytometry (FACS) Caliber (BD Bioscience, Mountain View, CA). Meanwhile, the treated cells were rinsed with PBS twice and fixed in 4% paraformaldehyde for 30 min. Then the fixed cells were stained with DAPI solution for 20 min and observed using LSM 710 confocal laser scanning microscope (CLSM, Carl Zeiss Microscopy LLC, Germany). In addition, to investigate the tumor-targeting ability of MDPAS micelles, the cells were incubated with AS1411 aptamer at a final concentration of 1 mM in advance and then treated with MDP and MDPAS micelles for 6 h. Afterwards, FACS analysis and CLSM observation were conducted to evaluate the cellular uptake efficiency of micelles.

To further study the intracellular distribution of MDPAS micelles, HepG2 cells were incubated with MDPAS micelles for 12 h. After the removal of medium, the cells were fixed in 4% paraformaldehyde for 30 min and subsequently stained with LysoTracker™ Green and DAPI for 30 min to label lysosome and nucleus, respectively. Finally, the cells were rinsed with PBS twice and observed through CLSM.

## Determination of ABCG2 mRNA Expression

The expression of ABCG2 mRNA after the micelles' treatment was evaluated using qPCR. In brief, HepG2 cells were inoculated in 6-well plates at a density of  $2.5 \times 10^5$  cells/well and cultured overnight. Then the cells were incubated with different micelles containing 0.6 μM DOX for 48 h and lysed by TRazol Universal reagent to extract total RNA. cDNA was prepared through the reverse transcription from 1 μg of total RNA using PrimeScript™ RT-PCR kit, and further employed as a template for PCR amplification by SYBR® Premix Ex Taq™ kit. The qPCR reaction was conducted on an ABI 7500 Fast Real-Time PCR System (Life Science, Foster, CA) and analyzed through  $2^{-\Delta\Delta C_T}$  method. The primers of reference gene β-actin and ABCG2 were listed as follows:

β-Actin: forward: 5'-GGATCAGCAAGCAGGAGTAG-3';

reverse: 5'-CACCTTCACCGTTCCAGTTT-3'.

ABCG2: forward: 5'-GGGTTCTCTTCTTCTGACGACC-3';

reverse: 5'-CACCTTCACCGTTCCAGTTT-3'.

## Anti-Proliferative Effect of MDPAS Micelles

The anti-proliferative effect of MDPAS micelles was evaluated using the MTT assay in HepG2 cells. Briefly, the cells were seeded in 96-well plates at a density of  $1.0 \times 10^4$  cells/well and incubated at 37 °C for 12 h, which were then incubated with different micelles harboring 0.6 μM DOX. After the exposure for 48 h, 20 μL of MTT solution (5 mg/mL) in PBS was mixed with the cells in each well, and the incubation was performed for another 4 h. After removing the medium, the formed formazan crystals in the wells were thoroughly dissolved using 200 μL DMSO, and the absorbance at 492 nm was monitored using a GF-M3000 microplate reader (Shandong, China). The cell viability (%) was calculated as follows:

$$\text{Cell viability (\%)} = \frac{A_{\text{treated cells}} - A_{\text{blank}}}{A_{\text{untreated cells}} - A_{\text{blank}}}$$

## Cell Apoptosis and Cell Cycle Arrest Analysis

The cell apoptosis and cell cycle arrest were carried out to investigate the mechanism of anti-proliferative effect induced by MDPAS micelles. First, HepG2 cells were

seeded into 6-well plates at a density of  $2.5 \times 10^5$  cells/well, and further cultured at 37 °C overnight. Different micelles containing 1.0  $\mu$ M DOX were then added into each well, and the cells were harvested and rinsed with PBS three times after the treatment for 48 h. The Annexin V-FITC/PI staining procedure was conducted in the dark for 30 min based on the apoptosis detection kit's instructions, whereas the cells were treated with PI staining solution according to the cell cycle detection kit's protocol. Finally, the apoptosis and cell cycle arrest induced by MDPAS micelles were analyzed through 30,000 gated cells by FACS.

### Western Blotting Analysis

The cells were seeded into 6-well plates and incubated overnight, and then treated with different micelles as described in the section "Cell apoptosis and cell cycle arrest analysis". After the treatment for 48 h, the cells were harvested and lysed using RIPA buffer containing 1 mM phenylmethanesulfonyl fluoride. The protein concentration was quantified using the bicinchoninic acid detection kit. An equal amount of proteins was subjected to the 12% SDS-PAGE analysis, and the gel was transferred to polyvinylidene fluoride membrane through the electroblotting strategy (200 mA, 1.5 h). The membrane was subsequently incubated with the primary antibodies at 4 °C overnight and further treated with the HRP-conjugated secondary antibody at 25 °C for 1 h. Finally, the membrane was rinsed with PBST solution twice and visualized by ECL luminescence reagent, and the expression level of proteins was captured by Tanon 1600 gel imaging system (Shanghai, China).

### Anti-Proliferative Effect of MDPAS Micelles in 3D Tumor Spheroids

The HepG2 cells were seeded in a 24-well ultra-low adsorption plate at a density of  $3 \times 10^4$  cells/well and incubated at 37 °C for 4 days, achieving the construction of 3D tumor spheroids. The intact spheroids were selected and treated with different micelles containing 0.8  $\mu$ M DOX for 24 h. Afterwards, the spheroids were observed through CLSM along the Z-axis. The tumor spheroids after the treatment were then digested with 1 mL of trypsin solution (0.25%, w/v) to obtain cell suspension, which was incubated with Annexin V-FITC/PI staining solution in the apoptosis detection kit at 37 °C for 30 min and analyzed through FACS to detect the apoptotic effect.

### In vivo Anti-Cancer Efficacy of MDPAS Micelles

All the animal studies were conducted according to the "Guide for the Care and Use of Laboratory Animals" (eighth edition, International Publication No: 978-0-309-15400-0) and approved by the Institutional Animal Ethics Committee of Jilin University (license No. SCXK-(JI) 2014-0012). Female BALB/c-nude mice (6-7 weeks) were purchased from Vital River Laboratory Animal Technology Co. Ltd. (Beijing, China). The HepG2 cells were digested and re-suspended in PBS at a final amount of  $1.0 \times 10^7$  cells and subcutaneously injected into the right flank of an individual mouse to establish the xenografted tumor model. Once the tumor tissue was developed with an average volume of 100 mm<sup>3</sup>, the HepG2 tumor-bearing mice were randomly separated into different groups (n=6 in each group) and intravenously injected with free DOX, MDP micelles and MPDAS micelles once a week for 4 times, with an equal DOX dose of 3.0 mg/kg per mouse. The daily change of body weight and tumor size of mice was monitored at the same time each day. The tumor volume (V) was measured by an electronic caliper and calculated using the formula  $V=(a \times b^2) \times 0.5$ , in which a and b represent the length of long axis and short axis of the tumor, respectively.

### Histological Analysis

At 28 days post-administration, the HepG2-xenografted mice were sacrificed and dissected. Tumor tissues as well as major organs (heart, lung, liver, spleen and kidney) were harvested and fixed in 4% paraformaldehyde at 4 °C for 2 days. Then, the paraffin-embedded tissues were sectioned into slices of 20- $\mu$ m thickness, stained with hematoxylin and eosin (H&E), and observed on an Olympus IX71 fluorescence microscopy (Tokyo, Japan). The apoptotic cells in tumor tissues were determined by in situ TUNEL detection kit according to the manufacturer's protocol. To determine the Ki67 and ABCG2 expression in tumor tissues, the slices were treated with 0.2% Triton X-100 in PBS for 5 min and blocked with 5% goat serum for 2 h. Subsequently, the samples were incubated with primary antibodies at 4 °C overnight, and the HRP-conjugated secondary antibody was added into the samples. After the incubation at 25 °C for 1 h, the samples were observed through fluorescence microscopy. In addition, the expression of ABCG2 was analyzed at the mRNA level using qPCR as described in the section

“Determination of ABCG2 mRNA expression”, in which 1 g of tumor tissues were homogenized in TRazol Universal reagent at 4 °C (1000 rpm, 5 min) and then centrifuged at 120,000 rpm for 10 min (4 °C).

## In vivo Biodistribution of MDPAS Micelles

To detect the in vivo biodistribution of MDPAS micelles, the tumor-bearing mice were randomly divided into three groups (n=3 in each group) when tumor tissues reached an average size of 500 mm<sup>3</sup>, including free DOX, MDP and MDPAS micelles. Different micelles were injected into mice via the tail vein at a DOX dose of 8.0 mg/kg per mouse. The mice were sacrificed and observed at 1 h, 4 h and 24 h post-injection, followed by the collection of heart, liver, spleen, lung, kidney and tumor tissues. The fluorescence of mice and harvested tissues were analyzed through a Kodak In-Vivo FX PRO Imaging System (New Haven, CT).

## Statistical Analysis

Experiments were conducted for three times, and the data were presented as mean  $\pm$  standard deviation (SD). The statistical analysis was performed by Student's *t*-test and one-way analysis of variance (ANOVA), where *p* value <0.05 (\*) and *p* value <0.01 (\*\*) were considered to be the statistical significance.

## Results and Discussion

### Preparation and Characterization of MDPAS Micelles

In the past two decades, nanoparticles have gained great interest owing to their favorable properties including high capacity for drug loading, low systematic toxicity, ideal physical and chemical stability, and pharmaceutical improvement of drug properties, and thus they have been widely studied in a series of diseases such as tumors, neurodegenerative diseases and inflammatory bowel diseases.<sup>50–53</sup> In the present study, polymeric micelles including M, MDP and MDPAS were prepared according to the procedure in Scheme 1. Briefly, MDP micelles were constructed using DC-Chol, Mal-PEG<sub>5K</sub>-PLA<sub>21K</sub> and mPEG<sub>5K</sub>-PLA<sub>10K</sub> as carriers in an emulsion/solvent evaporation strategy, where DOX was physically incorporated into the hydrophobic layer and miR-519c plasmid was encapsulated into the hydrophilic core. The AS1411 aptamer was then conjugated on the surface of micelles through Michael addition reaction, obtaining the

tumor-targeted micelles MDPAS. The conjugation of AS1411 aptamer was determined using agarose gel electrophoresis (Figure S1). Obviously, a clear band could be observed in the free aptamer group, and no bands could be detected for MDPAS micelles, indicating that AS1411 aptamer has been successfully conjugated on the surface of micelles.

The morphology of polymeric micelles was visualized by TEM, as shown in Figure 1A and S2. Three micelles exhibited a uniform and spherical nanostructure with hydrodynamic diameter ranging from 240 to 300 nm. Meanwhile, a visible corona observed in micelles suggested that the micelles have been successfully formed with core/shell structure. Thus, the loading of hydrophobic DOX and hydrophilic miR-519c plasmid could be simultaneously achieved in MDPAS micelles. During the preparation of micelles, the first sonication was completed to form the W/O primary emulsion, and the second sonication aimed to the construction of W/O/W double emulsion, and thus the core/shell structure was formed after the solvent evaporation and centrifugation. Similar phenomenon has also been obtained in the previous reports which achieved the delivery of siRNA (mPEG-PLA and BHEM-Chol as carriers),<sup>54</sup> and Cas9 mRNA and guide RNA (PLGA, PEG-PLA and BHEM-Chol as carriers).<sup>55</sup> The EE and DL values of DOX and miR-519c plasmid in MDPAS micelles were listed in Table S1. Particularly, a high EE value of miR-519c plasmid could be realized (86.53%), which was attributed to the presence of hydrophilic core and the positively charged density of DC-Chol confining the diffusion of nucleic acids within MDPAS micelles. We also evaluated the storage stability of MDPAS micelles for 7 days by particle size and zeta potential measurements (Figure 1B and C). The hydrodynamic diameter values of M, MDP and MDPAS micelles were determined to be 240  $\pm$  4.99, 280  $\pm$  2.01 and 315  $\pm$  2.15 nm, respectively. Notably, the particle size of three micelles remained unchanged in 7 days, indicating that the micelles possessed good stability without the formation of large aggregates. In addition, all these micelles exhibited negatively charged state, and no substantial change of zeta potential was detected. Moreover, the Tyndall effect could be observed for the micelles after the storage for 60 days using a visible optical path, suggesting the presence of stable micelles in the sample (Figure S3). Hence, MDPAS micelles was identified to possess favorable stability, which was beneficial to achieve the long-term storage and in vivo therapeutic applications.

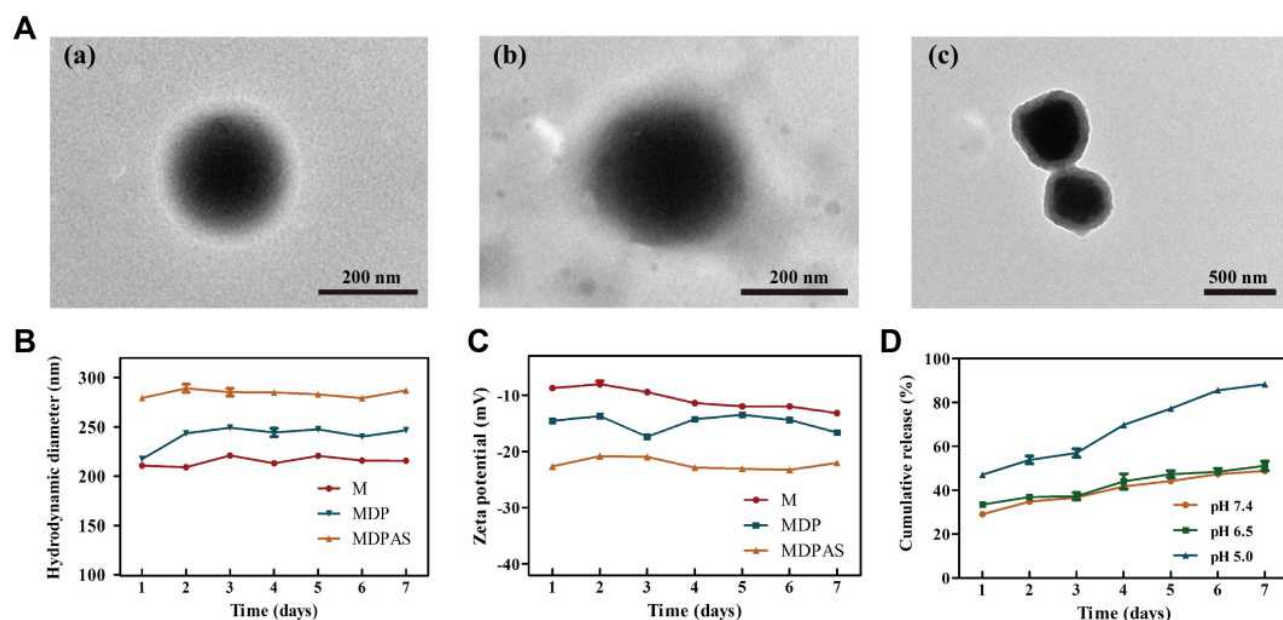


**Figure 1** Characterization and DOX release profile of MDPAS micelles. **(A)** The TEM images of M (a), MDP (b) and MDPAS micelles (c). The hydrodynamic size **(B)** and zeta potential **(C)** change of micelles stored at 4 °C for 7 days. **(D)** The cumulative release of DOX from MDPAS micelles under different pH conditions. Data were presented as mean  $\pm$  SD of triplicate experiments.

Further, the DOX release profile from MDPAS micelles was examined in the simulated physiological environment of pH 7.4, tumor microenvironment of pH 6.5, and endosomal environment of pH 5.0 (Figure 1D). A sustained drug release in MDPAS micelles was achieved at pH of 7.4, with a cumulative drug release of 49.98% after 7 days. In contrast, the DOX release from micelles showed a faster release pattern at pH of 5.0 (DOX release of 88.71% after 7 days). As ester bonds in the carriers Mal-PEG<sub>5K</sub>-PLA<sub>21K</sub> and mPEG<sub>5K</sub>-PLA<sub>10K</sub> were pH-sensitive, faster drug release could be achieved in MDPAS micelles at pH of 5.0. These results indicated that MDPAS micelles exhibited a controlled release of drugs in a pH-dependent manner, which was potential to obtain the rapid drug release and accumulation in the tumor tissue.

## Intracellular Uptake and Distribution of MDPAS Micelles

To confirm the AS1411-targeting ability of MDPAS micelles, we first compared the expression of nucleolin on the membrane of different cells using immunofluorescence analysis. As shown in Figure S4, nucleolin was barely expressed in normal cells such as L02 and NIH3T3. In contrast, obvious over-expression of nucleolin was achieved in cancer cells, implying that the abnormal

expression of nucleolin was a potential biomarker for the cancer diagnosis. As the highest expression of nucleolin was detected in HepG2 cells, the cellular uptake studies of MDPAS micelles were conducted using HepG2 and L02 cells through FACS and CLSM. In comparison to free DOX and MDP micelles, MDPAS micelles exhibited higher cellular uptake in HepG2 cells by FACS analysis (Figure 2A), indicating that AS1411 aptamer could enhance the cellular uptake efficiency of micelles by the favorable recognition ability towards nucleolin. However, the cellular uptake efficiency of MDPAS micelles decreased significantly when the cells were treated with AS1411 aptamer in advance. This phenomenon suggested that the pretreatment with aptamer could inhibit the endocytosis of MDPAS micelles by blocking the nucleolin expressed on the surface of HepG2 cells, therefore revealing that the internalization of MDPAS micelles in HepG2 cells was performed in an AS1411 aptamer-mediated endocytic pathway. Conversely, the pre-treatment with AS1411 aptamer had almost no influence on the endocytosis of MDPAS micelles in L02 cells, owing to the lower expression of nucleolin on L02 cells (Figure 2B). The internalization of micelles was further investigated in HepG2 and L02 cells through CLSM (Figures S5 and S6). There was no significant change of cellular uptake in HepG2 cells for the treatment with MDP micelles regardless of the pre-treatment with AS1411 aptamer. In

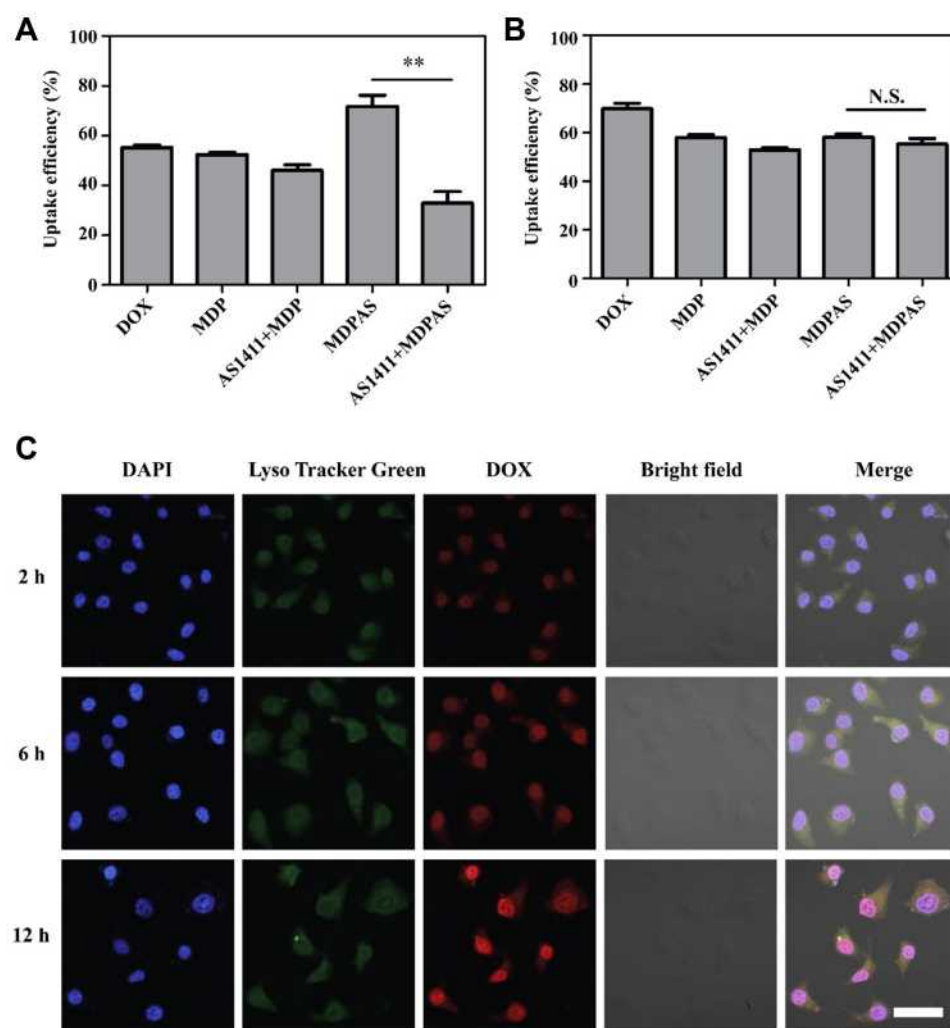


**Figure 2** Cellular uptake and intracellular distribution of MDPAS micelles. The cellular uptake efficiency of different formulations in HepG2 (**A**) and L02 cells (**B**) through FACS analysis (\*\* $p < 0.01$ ). (**C**) The CLSM images for the intracellular distribution of MDPAS micelles in HepG2 cells after the incubation for 2, 6 and 12 h, respectively. Blue (DAPI, nucleus), green (LysoTracker Green, lysosome) and red (DOX). Scale bar: 50  $\mu$ m.

**Abbreviation:** N.S., no significance.

contrast, the red fluorescence intensity could be dramatically reduced when the cells were pre-treated with AS1411 aptamer prior to the transfection with MDPAS micelles, indicating that the aptamer pre-treatment inhibited the intracellular delivery of MDPAS micelles. In L02 cells, similar red fluorescence intensity could be achieved in MDP and MDPAS groups, and the pre-treatment of AS1411 aptamer did not influence the DOX fluorescence in cytosol. These results revealed that the conjugation of AS1411 aptamer on the micelles could improve the intracellular delivery efficiency of nanoparticles in cancer cells in an AS1411 aptamer-dependent internalization pathway.

Subsequently, the lysosomal escape ability of MDPAS micelles was evaluated by CLSM (Figure 2C). Obviously, red fluorescence could be detected during the first 2 h,

indicating that MDPAS micelles could be successfully uptake by HepG2 cells. After the incubation for 6 h, red and green fluorescence was obviously overlapped and a large area of yellow fluorescence could be observed, suggesting that MDPAS micelles were mainly entrapped in the lysosomes. Clearly, stronger red fluorescence could be obtained after 12 h which did not overlap with green fluorescence, demonstrating that MDPAS micelles could successfully realize the endosomal escape. Besides, MDPAS micelles exhibited a high accumulation in the nucleus, which was caused by the targeting ability of AS1411 aptamer to the nucleolin expressed on the nucleus. In conclusion, these results revealed that MDPAS micelles possessed favorable cellular internalization and lysosomal escape ability, further enhancing the co-delivery efficiency of DOX and miR-519c plasmid.

## Reversing MDR Through the Inhibition of ABCG2

To verify whether MDR could be reversed by the inhibition of ABCG2, the intracellular DOX concentration and the ABCG2 expression level were detected by LC-MS/MS, qPCR and Western blotting, respectively. As shown in Figure 3A, blank micelle M and free DOX could not inhibit the expression of ABCG2 by qPCR analysis, whereas the micelles harboring miR-519c plasmid (MDP and MDPAS) dramatically decreased the expression of ABCG2 at the mRNA level. Notably, compared with MDP, MDPAS micelles achieved a higher inhibition of ABCG2 expression, which was mainly caused by the enhanced delivery efficiency from AS1411 aptamer-targeting ability. Consistently, Western blotting analysis showed that MDP and MDPAS micelles significantly decreased the ABCG2 expression at the protein level, and higher inhibition ability was obtained in the cells after the treatment with MDPAS micelles (Figure 3B and C). All these results elucidated that the delivery of miR-519c plasmid could efficiently achieve the knockdown of ABCG2. Further, the intracellular DOX concentration

after the micelles' treatment was explored by LC-MS/MS (Figure 3D). In comparison to the micelles without miR-519c plasmid, MDP and MDPAS micelles could greatly improve the intracellular DOX concentration after the treatment for 48 h, which was relied on the blockade of ABCG2-dependent drug efflux by miR-519c. These results demonstrated that MDPAS micelles containing miR-519c plasmid could reverse MDR by inhibiting the ABCG2 expression and decrease the resistance of cancer cells to chemotherapeutics. Thus, the co-delivery of DOX and miR-519c plasmid could facilitate the intracellular accumulation of DOX and potentially achieve a synergistic anti-cancer effect.

## In vitro Anti-Proliferative Effect of MDPAS Micelles

To evaluate the anti-proliferative effect of MDPAS micelles, the cell viability after the micelles' treatment was evaluated by MTT assay. As illustrated in Figure 4A, blank micelle M exhibited limited cytotoxicity in HepG2 cells, owing to the favorable biocompatibility of PEG-PLA and DC-Chol. Compared with free DOX, MDP

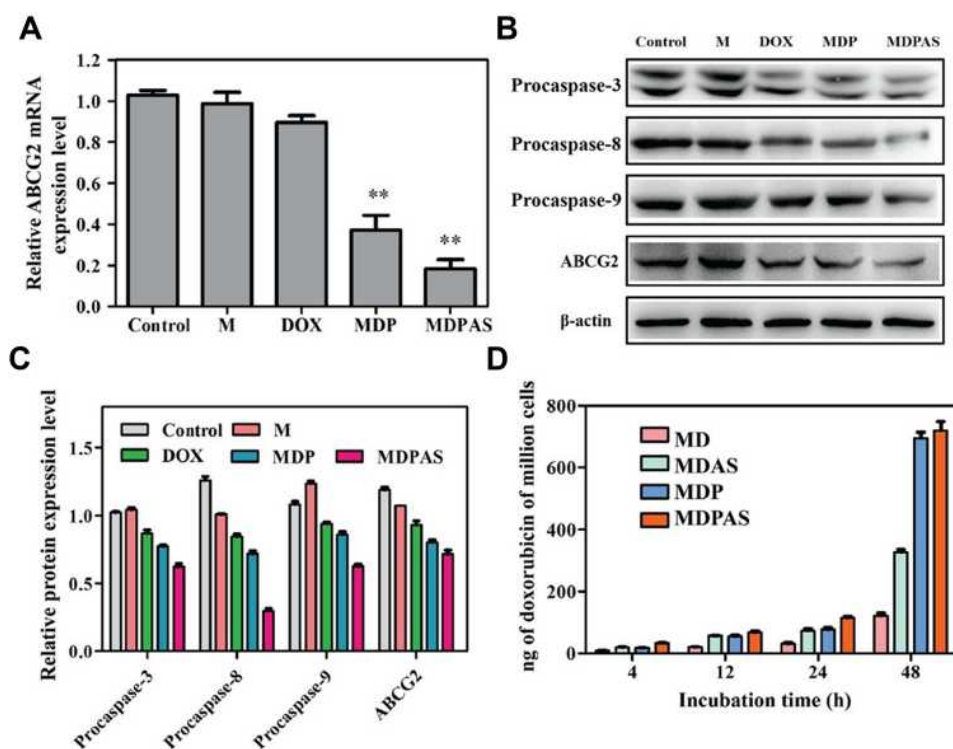


**Figure 3** Expression level of ABCG2 and apoptosis-related proteins. (A) The ABCG2 expression level in HepG2 cells after the treatment with different formulations through qPCR analysis (\*\* $p < 0.01$ , vs control group). (B) Western blotting analysis and the quantitative results (C) of procaspase-3, -8 and -9 and ABCG2 expression in HepG2 cells after the treatment with different formulations. (D) The intracellular DOX concentration in HepG2 cells after the treatment with micelles for different time by LC-MS/MS analysis.

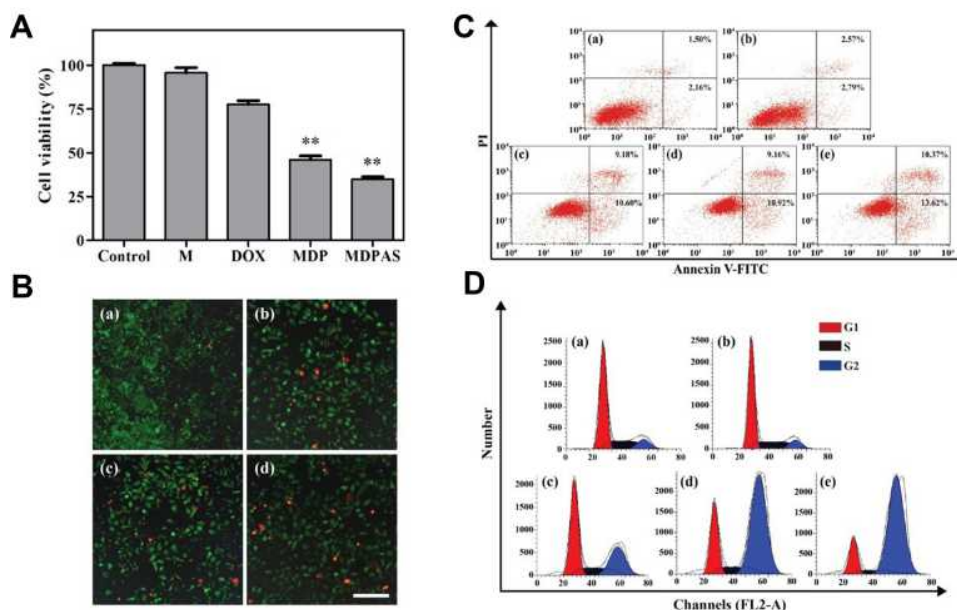


**Figure 4** Anti-proliferative effect of MDPAS micelles. **(A)** The cell viability of HepG2 cells after the treatment with different micelles by MTT assay (\*\* $p < 0.01$ , vs control group). **(B)** Live/Dead cell staining assay of HepG2 cells treated with control (a), free DOX (b), MDP (c) and MDPAS micelles (d), respectively. Scale bar: 200  $\mu\text{m}$ . **(C and D)** FACS analysis of the cell apoptosis and cell cycle arrest of HepG2 cells treated with control (a), M (b), free DOX (c), MDP (d) and MDPAS micelles (e).

and MDPAS micelles exhibited evident inhibition of cell proliferation, with cell viability of 47.80% and 36.30%, respectively. This phenomenon was mainly caused by the improved DOX accumulation in tumor cells due to the inhibition of ABCG2 drug efflux transporter by miR-519c. Notably, stronger anti-proliferative effect could be achieved in MDPAS micelles than MDP group, attributing to their efficient cellular uptake mediated by the targeting ability of AS1411 aptamer. Further, the proliferative inhibition of MDPAS micelles was measured by Live/Dead cell staining assay, in which live and dead cells generated green and red fluorescence, respectively. As shown in Figure 4B, more cells with red fluorescence were visualized in MDPAS group than those treated with free DOX and MDP micelles, indicating that MDPAS micelles could induce higher anti-proliferative effect in HepG2 cells. These data were consistent with the MTT assay, revealing that MDPAS micelles could achieve an improved inhibition ability of cell proliferation due to the high intracellular DOX concentration from efficient endocytosis of nanoparticles and suppression of MDR.

To assay the anti-proliferative mechanism of MDPAS micelle, we conducted the cell apoptosis and cell cycle distribution after the micelles' treatment by FACS analysis. As shown in Figure 4C, no apparent apoptosis was obtained in HepG2 cells after the treatment with blank micelle M, while free DOX induced obvious cell apoptosis

with apoptotic ratio of 19.78%. In contrast, MDPAS micelles could improve the apoptotic ratio to 23.99% which was relied on the enhanced intracellular DOX concentration through the suppression of MDR effect by miR-519c. To analyze the apoptotic mechanism triggered by MDPAS micelles, the expression of apoptosis-related caspases was determined by Western blotting analysis (Figure 3B). Compared with blank micelle, the procaspase-3 expression decreased significantly in the case of MDP and MDPAS micelles, with the lowest expression in the MDPAS treatment group. These results showed that MDPAS micelles could initiate the apoptosis by the activation of caspase-3. Meanwhile, compared with free DOX, the micelles MDP and MDPAS could efficiently suppress the expression of both procaspase-8 and procaspase-9, implying the activation of caspase-8 and caspase-9 by these two micelles. Consistently, the relative activity analysis of caspase-3, -8 and -9 also demonstrated the activation of these apoptosis-related proteins after the treatment with MDPAS micelles (Figure S7). In the apoptotic pathways, caspase-8 has been identified to execute the cell death receptor-mediated apoptosis, whereas the activation of caspase-9 has been considered as the initiator of mitochondria-dependent apoptosis signaling pathway.<sup>56</sup> The data implied that both apoptotic routes could be activated by MDPAS micelles, thereby leading to the anti-proliferative effect in cancer cells.

Next, the effect of MDPAS micelles on the cell cycle distribution was conducted by PI staining, followed by FACS analysis (Figure 4D and S8). Compared with the untreated cells, free DOX could induce the cell cycle arrest at G2 phase with a ratio of 30.93%, owing to the inhibition of topoisomerase by DOX in the DNA synthesis process. In contrast, the cells treated with MDP and MDPAS micelles exhibited larger proportion of cells at G2 phase (65.45% and 78.35%), indicating that the co-delivery of DOX and miR-519c could induce the cell cycle arrest at G2 phase leading to the inhibition of cell proliferation in a synergistic mode. Taken together, our results suggested that MDPAS micelles harboring DOX and miR-519c could be successfully uptake by HepG2 cells through the AS1411 aptamer-dependent manner and induce the apoptosis and cell cycle arrest to achieve the anti-proliferative effect, indicating that the combinational therapy could facilitate the anti-cancer response in a synergistic pattern of two components.

### Anti-Cancer Effect of MDPAS Micelles in 3D Tumor Spheroids

In contrast to 2D cell culture, the employment of 3D tumor spheroids could mimic the solid tumors more closely by sharing similar features such as the spatial distribution of cells, extracellular matrix, cell adhesion, hypoxia and acidic microenvironment, which has been widely used in the evaluation of anti-tumor drug delivery systems.<sup>57</sup> Here, the internalization of MDPAS micelles was tested in 3D tumor spheroids derived from HepG2 cells (Figure 5A and B). The 3D reconstruction and serial Z-stacks demonstrated that free DOX were distributed on the surface of tumor spheroids. In contrast, more red fluorescence of MDP and MDPAS micelles was observed in the inner portion of spheroids, indicating that the micelles could facilitate the penetration by overcoming the inner pressure of spheroids. Particularly, MDPAS micelles were capable of diffusing and penetrating across multilayer cells due to the targeting ability, which was critical for achieving excellent anti-cancer efficacy. Subsequently, the treated tumor spheroids were digested into single-cell suspension which was directly employed to determine the ratio of apoptotic cells through FACS analysis. As shown in Figure 5C, compared with untreated cells (5.54%), higher apoptotic ratios were obtained in the treatment groups with free DOX and MDP micelles (9.66% and 10.64%). Moreover, the treatment with MDPAS micelles could

increase the proportion of apoptotic cells to 18.22% in 3D tumor spheroids, suggesting that the co-delivery of DOX and miR-519c by MDPAS micelles could achieve better therapeutic efficacy through the enhanced cellular uptake and deep penetration in tumor tissues.

### In vivo Biodistribution of MDPAS Micelles

Encouraged by the apparent anti-cancer effect of MDPAS micelles achieved in in vitro study, we established a tumor-xenografted mice model via the subcutaneous injection of HepG2 cells and then tracked the in vivo biodistribution of MDPAS micelles after 24 h post-intravenous injection. As shown in Figure 6 and S9, free DOX was accumulated in tumor tissues during the first 1 h and rapidly eliminated by the bloodstream. In contrast, stronger red fluorescence could be obtained in tumor tissues for the MDPAS micelles, implying that they possessed an excellent tumor-targeting ability and facilitated the tissue penetration of DOX and miR-519c in tumor sites. In addition, red fluorescence of MDPAS micelles still remained in the tumor after 24 h post-injection, while no visible fluorescence was shown in free DOX, indicating that MDPAS micelles could extend the retention time of DOX in tumors owing to the inhibition of MDR effect by miR-519c. Interestingly, except for the accumulation in liver, MDP and MDPAS micelles displayed the accumulation in lung following 4 h post-administration, which was probably caused by the non-specific phagocytosis of lung tissue. Thus, these results demonstrated that MDPAS micelles maintained the stability to prevent the quick elimination in the blood and also possessed an excellent tumor-targeting capacity, providing an efficient strategy for the co-delivery of DOX and miR-519c in the cancer treatment.

### In vivo Anti-Cancer Efficacy of MDPAS Micelles

To investigate the in vivo therapeutic efficacy of MDPAS micelles in cancer treatment, different formulations were injected to the HepG2-bearing mice via intravenous administration. The tumor growth profile was recorded for 28 days after the first intravenous injection of different formulations (Figure 7A). Rapid tumor growth was obtained in the control group, and blank micelle M showed no inhibitory effects on the tumor growth. Though free DOX and MDP micelles could reduce the tumor volume, MDPAS micelles exhibited more potent

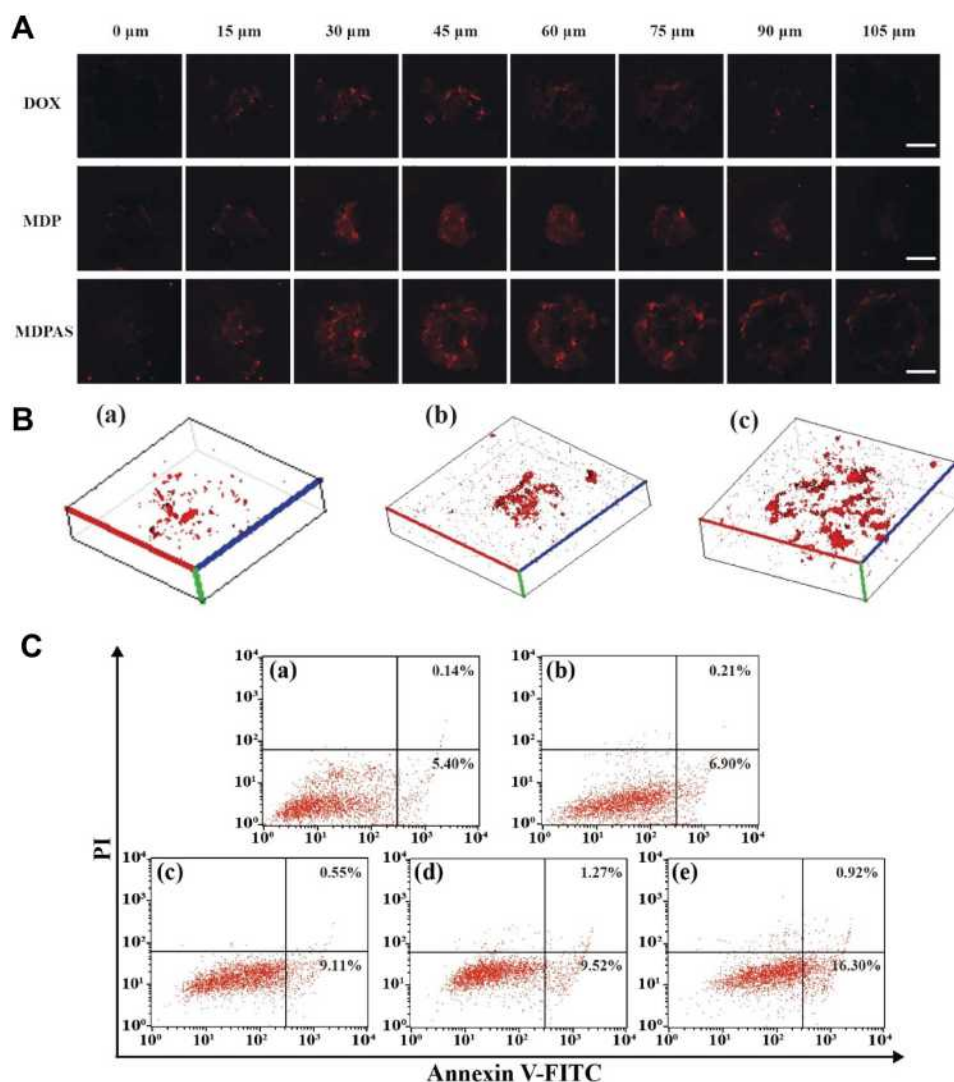


**Figure 5** Distribution and cell apoptosis in 3D tumor spheroids. **(A)** The CLSM images of 3D tumor spheroids treated with different micelles by scanning along the Z-axis. Scale bar: 50  $\mu\text{m}$ . **(B)** The 3D reconstruction of spheroids treated with free DOX (a), MDP (b) and MDPAS micelles (c), respectively. **(C)** FACS analysis for the cell apoptosis in 3D spheroids after the treatment with different formulations: control (a), M (b), free DOX (c), MDP (d) and MDPAS micelles (e).

inhibition of tumor growth, indicating that the co-delivery of DOX and miR-519c could realize a synergistic anti-cancer response. The increased therapeutic efficacy mediated by MDPAS micelles was mainly caused by the high delivery efficiency as well as the efficient suppression of MDR effect by miR-519c. Moreover, the tumor size after the MDPAS micelles' treatment was smaller than that of MDP group at the end of therapy (Figure 7B). These results suggested that the combinational therapy mediated by MDPAS micelles could efficiently inhibit the tumor growth, achieving an enhanced treatment efficacy through the synergistic effect of therapeutic drug and gene.

To further explore the anti-cancer effect of micelles, the paraffin-embedded tumor tissues of different treatment groups were sectioned into slices and analyzed by H&E

and immunohistochemical staining (Figure 7C). As shown in H&E staining images, an intact cellular structure could be observed in the control group, whereas the tumor tissues of mice treated with free DOX, MDP and MDPAS micelles exhibited obvious cell apoptosis evidenced by the pyknotic nuclei and incompact cytoplasm in the cells. Meanwhile, the apoptosis of tumor tissues was evaluated by TUNEL staining. The results demonstrated that the apoptosis of tumor cells could be triggered by the treatment with free DOX, MDP and MDPAS micelles, while the micelles containing DOX and miR-519c could induce more apoptotic cells than other two groups. Consistently, the Ki67 staining assay confirmed that merely few apoptotic cells were detected in tumor tissues obtained from control and blank micelle groups, and a reduced density of

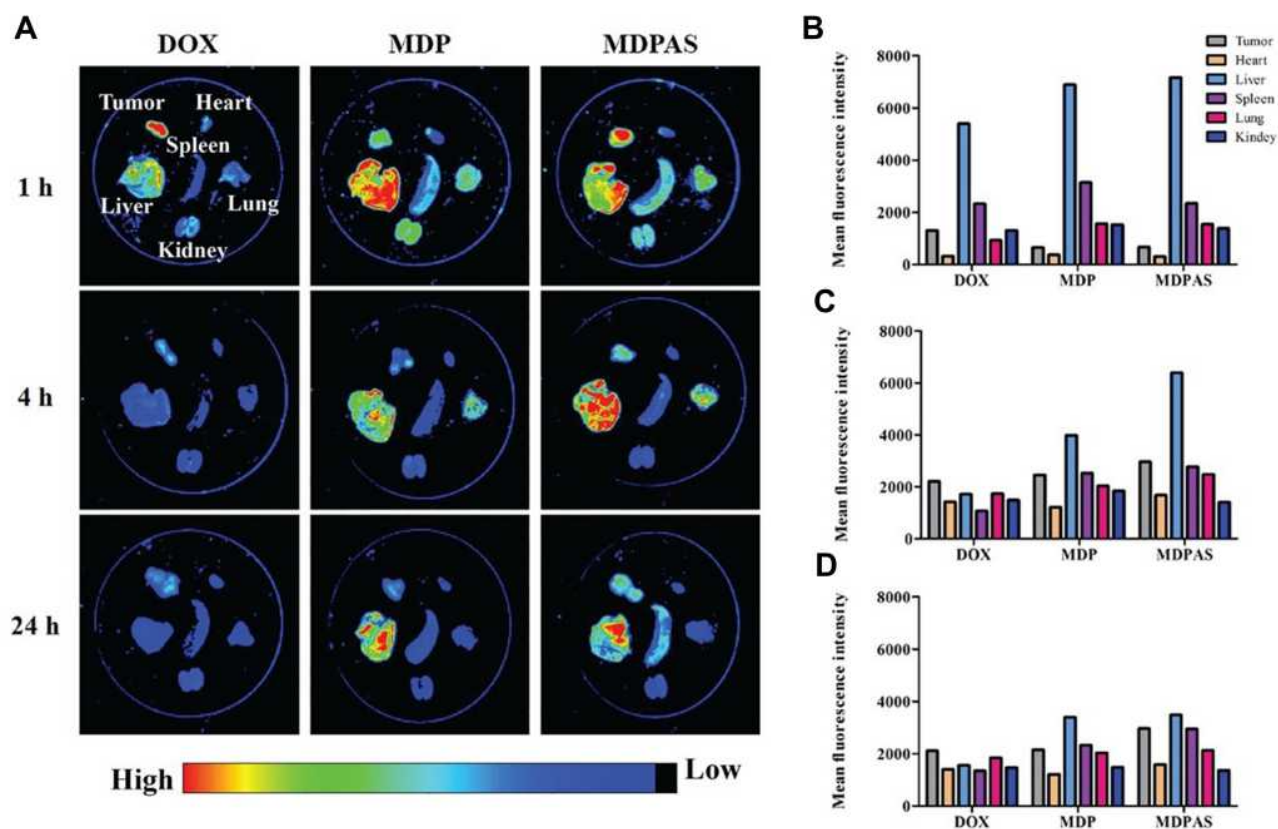


**Figure 6** Biodistribution analysis of MDPAS micelles. **(A)** In vivo biodistribution of micelles in different organs and tumor tissues (n=3 per group). **(B–D)** The mean fluorescence intensity of different organs and tumor tissues at 1, 4 and 12 h post-injection, respectively.

Ki67-staining cells could be clearly observed in tumor tissues after the treatment with DOX. Notably, lower Ki67 expression could be detected in tumor tissues treated with MDP and MDPAS micelles, suggesting that the micelles could significantly inhibit the cell proliferation and further lead to the tumor growth inhibition. The expression level of ABCG2 in tumor tissues was evaluated by immunohistochemical staining and qPCR (Figure 7C and S10). Compared with control and blank micelle M groups, the ABCG2 expression was dramatically improved after the treatment with free DOX. This phenomenon was probably caused by the fact that the sustained administration of DOX could induce the MDR effect to resist the therapeutic efficacy via the induction of ABCG2 over-expression. Nevertheless, the micelles could decrease the expression level of ABCG2 owing to the controlled release of DOX in the cytosol. Meanwhile, MDPAS micelles could down-regulate the ABCG2 expression more significantly, which would be beneficial to enhance the sensitivity of cancer cells to DOX and improve the anti-cancer response of nanomedicine. Our findings confirmed that the micelles-mediated co-delivery

of DOX and miR-519c could improve the therapeutic efficacy by the reversion of MDR effect.

## Biocompatibility Analysis of MDPAS Micelles

The biocompatibility of MDPAS micelles was analyzed by monitoring the body weight and the morphology of histological sections obtained from major organs. As shown in Figure S11, no significant change of body weight was achieved in the period of micelles' treatment in comparison to the control group, indicating that MDPAS micelles did not induce obvious systemic toxicity. Previous studies have confirmed that DOX is a cytotoxic drug which suffered from severe side effects such as cardiotoxicity.<sup>58–60</sup> Thus, the H&E staining analysis was performed for the major organs to evaluate whether the micelles containing DOX could cause the pathological changes of these organs (Figure 7D). Due to the favorable biocompatibility and biodegradability of PEG-PLA and DC-Chol, blank micelle exhibited good biocompatibility in mice with no toxicity to the organs. Moreover, there were no obvious pathological

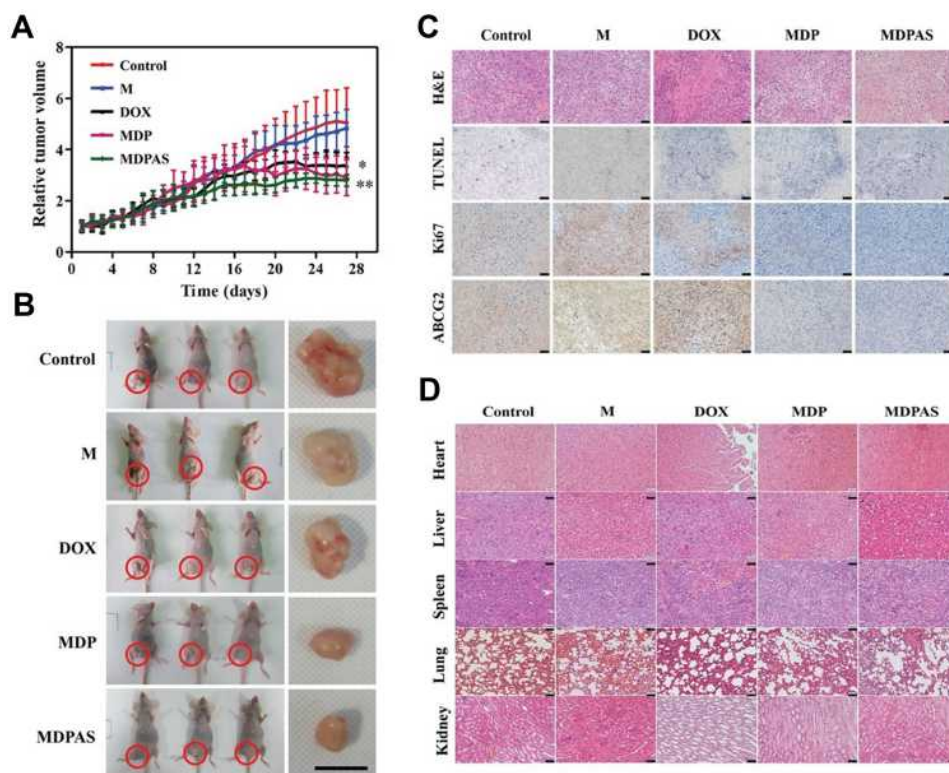


**Figure 7** In vivo anti-cancer efficacy and biocompatibility of MDPAS micelles. **(A)** The tumor volume profile of HepG2-xenografted nude mice after the treatment with different formulations ( $n=6$  per group,  $*p < 0.05$  and  $**p < 0.01$ , vs control group). **(B)** Representative images of excised tumor tissues from tumor-bearing mice received different treatments. Scale bar: 1 cm. **(C)** Representative images of H&E and immunohistochemical staining of tumor tissues. Scale bar: 100 nm. **(D)** Representative images of H&E staining of heart, liver, spleen, lung and kidney at 28 days post-administration. Scale bar: 100 nm.

lesions of major organs observed in MDP and MDPAS groups, suggesting that the encapsulation of DOX by micelles could reduce its systemic toxicity especially the cardiotoxicity. Overall, the MDPAS micelles provided a favorably biocompatible delivery system for chemotherapeutics and oligonucleotides, and thus exhibited great potential in the future biomedical applications.

## Conclusion

In summary, an AS1411 aptamer-modified micelle system was successfully developed based on PEG-PLA to realize the tumor-targeting co-delivery of DOX and miR-519c and the anti-cancer treatment in a synergistic pattern of two components. The MDPAS micelle has been demonstrated to possess prominent tumor-targeting ability via the specific recognition of nucleolin over-expressed on cancer cells and the efficient internalization in an AS1411 aptamer-dependent pathway. Meanwhile, the co-delivery of DOX and miR-519c by MDPAS micelle could reverse the MDR effect by inhibiting the ABCG2-dependent drug efflux and increasing the intracellular DOX concentration, which could facilitate the suppression of tumor growth and obtain

a desirable therapeutic efficacy in cancer treatment. Thus, the MDPAS micelle held a promise for the combination of chemotherapy and gene therapy, and provided a potential approach in cancer treatment especially for the tumors with strong drug resistance.

## Acknowledgments

The work was supported by the National Key R&D Program of China (2020YFA0907003), the National Natural Science Foundation of China (32071267, 81872928 and 32000897), the Science & Technology Department of Jilin Province (20190201288JC), the Development and Reform Commission of Jilin Province (2021C041-4) and the Graduate Innovation Program of Jilin University (101832020DJX032).

## Disclosure

The authors report no conflicts of interest in this work.

## References

1. El-Serag HB. Hepatocellular carcinoma. *N Engl J Med.* 2011; 365:1118–1127. doi:10.1056/NEJMra1001683

2. Sherman M, Kim RW, Dziura J. Risk scores for hepatocellular carcinoma in chronic hepatitis B. *Hepatology*. 2015;61:1784–1786. doi:10.1002/hep.27765
3. Liu Y, Tang Y, Wu J, et al. Facile synthesis of biodegradable flower-like hydroxyapatite for drug and gene delivery. *J Colloid Interface Sci*. 2020;570:402–410. doi:10.1016/j.jcis.2020.03.010
4. Ikeda M, Morizane C, Ueno M, et al. Chemotherapy for hepatocellular carcinoma: current status and future perspectives. *Jpn J Clin Oncol*. 2018;48:103–114. doi:10.1093/jjco/hyx180
5. Greten TF, Lai CW, Li G, et al. Targeted and immune-based therapies for hepatocellular carcinoma. *Gastroenterology*. 2019;156:510–524. doi:10.1053/j.gastro.2018.09.051
6. Cheng X, Zeng X, Zheng Y, et al. pH-sensitive pluronic micelles combined with oxidative stress amplification for enhancing multidrug resistance breast cancer therapy. *J Colloid Interface Sci*. 2020;565:254–269. doi:10.1016/j.jcis.2020.01.029
7. Lee WK, Thevenod F. Oncogenic PITX2 facilitates tumor cell drug resistance by inverse regulation of hOCT3/SLC22A3 and ABC drug transporters in colon and kidney cancers. *Cancer Lett*. 2019;449:237–251. doi:10.1016/j.canlet.2019.01.044
8. Wang F, Wang YC, Dou S, et al. Doxorubicin-tethered responsive gold nanoparticles facilitate intracellular drug delivery for overcoming multidrug resistance in cancer cells. *ACS Nano*. 2011;5:3679–3692. doi:10.1021/nn200007z
9. Fan YF, Zhang W, Zeng L, et al. Dacomitinib antagonizes multidrug resistance (MDR) in cancer cells by inhibiting the efflux activity of ABCB1 and ABCG2 transporters. *Cancer Lett*. 2018;421:186–198. doi:10.1016/j.canlet.2018.01.021
10. Zhang L, Li Y, Wang Q, et al. The PI3K subunits, P110 $\alpha$  and P110 $\beta$  are potential targets for overcoming P-gp and BCRP-mediated MDR in cancer. *Mol Cancer*. 2020;19:10. doi:10.1186/s12943-019-1112-1
11. Chol KY, Silvestre OF, Huang X, et al. Versatile RNA interference nanoplatform for systemic delivery of RNAs. *ACS Nano*. 2014;8:4559–4570. doi:10.1021/nn500085k
12. Orlando BJ, Liao M. ABCG2 transports anticancer drugs via a closed-to-open switch. *Nat Commun*. 2020;11:2264. doi:10.1038/s41467-020-16155-2
13. Brackman DJ, Giacomini KM. Reverse translational research of ABCG2 (BCRP) in human disease and drug response. *Clin Pharmacol Ther*. 2018;103:233–242. doi:10.1002/cpt.903
14. Furedi A, Szebenyi K, Toth S, et al. Pegylated liposomal formulation of doxorubicin overcomes drug resistance in a genetically engineered mouse model of breast cancer. *J Control Release*. 2017;261:287–296. doi:10.1016/j.jconrel.2017.07.010
15. Lu TX, Rothenberg ME. MicroRNA. *J Allergy Clin Immunol*. 2018;141(4):1202–1207. doi:10.1016/j.jaci.2017.08.034
16. Maiti C, Parida S, Kayal S, et al. Redox-responsive core-cross-linked block copolymer micelles for overcoming multidrug resistance in cancer cells. *ACS Appl Mater Interfaces*. 2018;10:5318–5330. doi:10.1021/acsami.7b18245
17. Bayraktar R, van Roosbroeck K. MiR-155 in cancer drug resistance and as target for miRNA-based therapeutics. *Cancer Metastasis Rev*. 2018;37:33–44. doi:10.1007/s10555-017-9724-7
18. Iyer AK, Duan Z, Amiji MM. Nanodelivery systems for nucleic acid therapeutics in drug resistant tumors. *Mol Pharm*. 2014;11:2511–2526. doi:10.1021/mp500024p
19. To KK, Leung WW, Ng SS. Exploiting a novel miR-519c-HuR-ABCG2 regulatory pathway to overcome chemoresistance in colorectal cancer. *Exp Cell Res*. 2015;338:222–231. doi:10.1016/j.yexcr.2015.09.011
20. Cha ST, Chen PS, Johansson G, et al. MicroRNA-519c suppresses hypoxia-inducible factor-1 $\alpha$  expression and tumor angiogenesis. *Cancer Res*. 2010;70:2675–2685. doi:10.1158/0008-5472.CAN-09-2448
21. To KK, Robey RW, Knutsen T, et al. Escape from hsa-miR-519c enables drug-resistant cells to maintain high expression of ABCG2. *Mol Cancer Ther*. 2009;8:2959–2968. doi:10.1158/1535-7163.MCT-09-0292
22. Wu D, Wang C, Yang J, et al. Improving the intracellular drug concentration in lung cancer treatment through the codelivery of doxorubicin and miR-519c mediated by porous PLGA microparticle. *Mol Pharm*. 2016;13:3925–3933. doi:10.1021/acs.molpharmaceut.6b00702
23. Rao J, Mei L, Liu J, et al. Size-adjustable micelles co-loaded with a chemotherapeutic agent and an autophagy inhibitor for enhancing cancer treatment via increased tumor retention. *Acta Biomater*. 2019;89:300–312. doi:10.1016/j.actbio.2019.03.022
24. Wei X, Liao J, Dovoudi Z, et al. Folate receptor-targeted and GSH-responsive carboxymethyl chitosan nanoparticles containing covalently entrapped 6-mercaptopurine for enhanced intracellular drug delivery in leukemia. *Mar Drugs*. 2018;16:439. doi:10.3390/md16110439
25. Liao J, Peng H, Wei X, et al. A bio-responsive 6-mercaptopurine/doxorubicin based “Click Chemistry” polymeric prodrug for cancer therapy. *Mater Sci Eng C*. 2020;108:110461. doi:10.1016/j.msec.2019.11.0461
26. Liao J, Peng H, Liu C, et al. Dual pH-responsive-charge-reversal micelle platform for enhanced anticancer therapy. *Mater Sci Eng C*. 2021;118:111527. doi:10.1016/j.msec.2020.11.1527
27. Yang Z, Gao D, Cao Z, et al. Drug and gene co-delivery systems for cancer treatment. *Biomater Sci*. 2015;3:1035–1049. doi:10.1039/C4BM00369A
28. Yang J, Arya S, Lung P, et al. Hybrid nanovaccine for the co-delivery of the mRNA antigen and adjuvant. *Nanoscale*. 2019;11:21782–21789. doi:10.1039/C9NR05475H
29. Chen Q, Xu M, Zheng W, et al. Se/Ru-decorated porous metal-organic framework nanoparticles for the delivery of pooled siRNAs to reversing multidrug resistance in Taxol-resistant breast cancer cells. *ACS Appl Mater Interfaces*. 2017;9:6712–6724. doi:10.1021/acsami.6b12792
30. Zhang H, Zhang J, Li Q, et al. Site-specific MOF-based immunotherapeutic nanoplatforms via synergistic tumor cells-targeted treatment and dendritic cells-targeted immunomodulation. *Biomaterials*. 2020;245:119983. doi:10.1016/j.biomaterials.2020.119983
31. Tian H, Zhang M, Jin G, et al. Cu-MOF chemodynamic nanoplatform via modulating glutathione and H<sub>2</sub>O<sub>2</sub> in tumor microenvironment for amplified cancer therapy. *J Colloid Interface Sci*. 2021;587:359–366. doi:10.1016/j.jcis.2020.12.028
32. Zhou Y, Ren X, Hou Z, et al. Engineering a photosensitizer nanoplatform for amplified photodynamic immunotherapy via tumor microenvironment modulation. *Nanoscale Horiz*. 2021;6:121–130. doi:10.1039/D0NH00480D
33. Ren X, Wang N, Zhou Y, et al. An injectable hydrogel using an immunomodulating gelator for amplified tumor immunotherapy by blocking the arginase pathway. *Acta Biomater*. 2021. doi:10.1016/j.actbio.2021.01.041
34. Wan X, Beaudoin JJ, Vinod N, et al. Co-delivery of paclitaxel and cisplatin in poly(2-oxazoline) polymeric micelles: implications for drug loading, release, pharmacokinetics and outcome of ovarian and breast cancer treatments. *Biomaterials*. 2019;192:1–14. doi:10.1016/j.biomaterials.2018.10.032
35. Upponi JR, Jerajani K, Nagesha DK, et al. Polymeric micelles: theranostic co-delivery system for poorly water-soluble drugs and contrast agents. *Biomaterials*. 2018;170:26–36. doi:10.1016/j.biomaterials.2018.03.054
36. Yang Y, Meng Y, Ye J, et al. Sequential delivery of VEGF siRNA and paclitaxel for PVN destruction, anti-angiogenesis, and tumor cell apoptosis procedurally via a multi-functional polymer micelle. *J Control Release*. 2018;287:103–120. doi:10.1016/j.jconrel.2018.08.028
37. Hu R, Zheng H, Cao J, et al. Self-assembled hyaluronic acid nanoparticles for pH-sensitive release of doxorubicin: synthesis and in vitro characterization. *J Biomed Nanotechnol*. 2017;13:1058–1068. doi:10.1166/jbn.2017.2406

38. Daman Z, Montazeri H, Azizi M, et al. Polymeric micelles of PEG-PLA copolymer as a carrier for salinomycin against gemcitabine-resistant pancreatic cancer. *Pharm Res.* 2015;32:3756–3767. doi:10.1007/s11095-015-1737-8
39. Dou S, Yang X, Xiong M, et al. ScFv-decorated PEG-PLA-based nanoparticles for enhanced siRNA delivery to Her2<sup>+</sup> breast cancer. *Adv Healthcare Mater.* 2014;3:1792–1803. doi:10.1002/adhm.201400037
40. Shi Y, Huang W, Liang R, et al. Improvement of in vivo efficacy of recombinant human erythropoietin by encapsulation in PEG-PLA micelle. *Int J Nanomed.* 2013;8:1–11.
41. Zheng H, Yin L, Zhang X, et al. Redox sensitive shell and core crosslinked hyaluronic acid nanocarriers for tumor-targeted drug delivery. *J Biomed Nanotechnol.* 2016;12:1641–1653. doi:10.1166/jbn.2016.2279
42. Phan QT, Le MH, Le TTH, et al. Characteristics and cytotoxicity of folate-modified curcumin-loaded PLA-PEG micellar nano systems with various PLA:PEG ratios. *Int J Pharm.* 2016;507(1–2):32–40. doi:10.1016/j.ijpharm.2016.05.003
43. Khan AR, Yang X, Fu M, et al. Recent progress of drug nanoformulations targeting to brain. *J Control Release.* 2018;291:37–64.
44. Zhang D, Zhang J. Surface engineering of nanomaterials with phospholipid-polyethylene glycol-derived functional conjugates for molecular imaging and targeted therapy. *Biomaterials.* 2020;230:119646. doi:10.1016/j.biomaterials.2019.119646
45. Zhu G, Chen X. Aptamer-based targeted therapy. *Adv Drug Deliver Rev.* 2018;134:65–78. doi:10.1016/j.addr.2018.08.005
46. Alshaer W, Hillaireau H, Fattal E. Aptamer-guided nanomedicines for anticancer drug delivery. *Adv Drug Deliver Rev.* 2018;134:122–137. doi:10.1016/j.addr.2018.09.011
47. Deng R, Shen N, Yang Y, et al. Targeting epigenetic pathway with gold nanoparticles for acute myeloid leukemia therapy. *Biomaterials.* 2018;167:80–90. doi:10.1016/j.biomaterials.2018.03.013
48. Wu J, Song C, Jiang C, et al. Nucleolin targeting AS1411 modified protein nanoparticle for antitumor drugs delivery. *Mol Pharm.* 2013;10:3555–3563. doi:10.1021/mp300686g
49. Mosafer J, Teymouri M, Abnous K, et al. Study and evaluation of nucleolin-targeted delivery of magnetic PLGA-PEG nanospheres loaded with doxorubicin to C6 glioma cells compared with low nucleolin-expressing L929 cells. *Mater Sci Eng C Mater Biol Appl.* 2017;72:123–133. doi:10.1016/j.msec.2016.11.053
50. Hu R, Zheng H, Cao J, et al. Synthesis and in vitro characterization of carboxymethyl chitosan-CBA-doxorubicin conjugate nanoparticles as pH-sensitive drug delivery systems. *J Biomed Nanotechnol.* 2017;13:1097–1105. doi:10.1166/jbn.2017.2407
51. Poovaiah N, Davoudi Z, Peng H, et al. Treatment of neurodegenerative disorders through the blood-brain barrier using nanocarriers. *Nanoscale.* 2018;10:16962–16983. doi:10.1039/C8NR04073G
52. Davoudi Z, Peroutka-Bigus N, Bellaire B, et al. Intestinal organoids containing poly(lactic-co-glycolic acid) nanoparticles for the treatment of inflammatory bowel diseases. *J Biomed Mater Res A.* 2018;106:876–886. doi:10.1002/jbm.a.36305
53. Yang B, Jiang J, Jiang L, et al. Chitosan mediated solid lipid nanoparticles for enhanced liver delivery of zedoary turmeric oil in vivo. *Int J Biol Macromol.* 2020;149:108–115. doi:10.1016/j.ijbiomac.2020.01.222
54. Yang X, Dou S, Sun T, et al. Systemic delivery of siRNA with cationic lipid assisted PEG-PLA nanoparticles for cancer therapy. *J Control Release.* 2011;156:203–211. doi:10.1016/j.jconrel.2011.07.035
55. Xu C, Lu Z, Luo Y, et al. Targeting of NLRP3 inflammasome with gene editing for the amelioration of inflammatory diseases. *Nat Commun.* 2018;9:4092. doi:10.1038/s41467-018-06522-5
56. Yang J, Zhang J, Xing J, et al. Inhibition of proliferation and migration of tumor cells through phenylboronic acid-functionalized polyamidoamine-mediated delivery of a therapeutic DNase Dnase13. *Int J Nanomed.* 2019;14:6371–6385. doi:10.2147/IJN.S211744
57. Huang B, Gao J. Application of 3D cultured multicellular spheroid tumor models in tumor-targeted drug delivery system research. *J Control Release.* 2018;270:246–259. doi:10.1016/j.jconrel.2017.12.005
58. Gupta SK, Garg A, Bar C, et al. Quaking inhibits doxorubicin-mediated cardiotoxicity through regulation of cardiac circular RNA expression. *Circ Res.* 2018;122:246–254. doi:10.1161/CIRCRESAHA.117.311335
59. Zhao L, Tao X, Qi Y, et al. Protective effect of dioscin against doxorubicin-induced cardiotoxicity via adjusting microRNA-140-5p-mediated myocardial oxidative stress. *Redox Biol.* 2018;16:189–198. doi:10.1016/j.redox.2018.02.026
60. Hu X, Dong M, Liang X, et al. Reactive oxygen species-mediated inflammation and apoptosis in hand-foot syndrome induced by PEGylated liposomal doxorubicin. *Int J Nanomed.* 2021;16:471–480. doi:10.2147/IJN.S280187

## International Journal of Nanomedicine

### Publish your work in this journal

The International Journal of Nanomedicine is an international, peer-reviewed journal focusing on the application of nanotechnology in diagnostics, therapeutics, and drug delivery systems throughout the biomedical field. This journal is indexed on PubMed Central, MedLine, CAS, SciSearch®, Current Contents®/Clinical Medicine,

Journal Citation Reports/Science Edition, EMBase, Scopus and the Elsevier Bibliographic databases. The manuscript management system is completely online and includes a very quick and fair peer-review system, which is all easy to use. Visit <http://www.dovepress.com/testimonials.php> to read real quotes from published authors.

Submit your manuscript here: <https://www.dovepress.com/international-journal-of-nanomedicine-journal>

Dovepress